Editors' Suggestion

Intrinsic Correlation between the Fraction of Liquidlike Zones and the β Relaxation in High-Entropy Metallic Glasses

Y. J. Duan,[1,2] L. T. Zhang,[1] J. C. Qiao,[1,*] Yun-Jiang Wang,[3,4] Y. Yang,[5,6] T. Wada,[7] H. Kato,[7] J. M. Pelletier,[8] E. Pineda,[2,†] and D. Crespo[2]

[1]School of Mechanics, Civil Engineering and Architecture, Northwestern Polytechnical University, Xi'an 710072, China
[2]Department of Physics, Institute of Energy Technologies, Universitat Politècnica de Catalunya, Barcelona 08019, Spain
[3]State Key Laboratory of Nonlinear Mechanics, Institute of Mechanics, Chinese Academy of Sciences, Beijing 100190, China
[4]School of Engineering Science, University of Chinese Academy of Sciences, Beijing 100049, China
[5]Department of Mechanical Engineering, College of Engineering, City University of Hong Kong, Tat Chee Avenue, Kowloon Tong, Kowloon, Hong Kong SAR, China
[6]Department of Materials Science and Engineering, College of Engineering, City University of Hong Kong, Tat Chee Avenue, Kowloon Tong, Kowloon, Hong Kong SAR, China
[7]Institute for Materials Research, Tohoku University, Sendai 980-8577, Japan
[8]Université de Lyon, MATEIS, UMR CNRS5510, Bâtiment B. Pascal, INSA-Lyon, F-69621 Villeurbanne Cedex, France

(Received 11 November 2021; revised 21 June 2022; accepted 16 September 2022; published 20 October 2022)

Lacking the structural information of crystalline solids, the origin of the relaxation dynamics of metallic glasses is unclear. Here, we report the evolution of stress relaxation of high-entropy metallic glasses with distinct β relaxation behavior. The fraction of liquidlike zones, determined at each temperature by the intensity of stress decay, is shown to be directly related to both the aging process and the spectrum of relaxation modes obtained by mechanical spectroscopy. The results shed light on the intrinsic correlation between the static and dynamic mechanical response in high-entropy and conventional metallic glasses, pointing toward a sluggish diffusion high-entropy effect in the liquid dynamics.

DOI: 10.1103/PhysRevLett.129.175501

Owing to the disordered atomic structure, metallic glasses (MGs) show unique properties [1–4]. Besides, high-entropy alloys (HEAs), containing equimolar concentrations of each component, have been developed recently [5–7]. Benefiting from the high configurational entropy, large lattice distortion, sluggish diffusion, and the cocktail effect [8,9], HEAs exhibit distinctive physical and mechanical properties [5,9,10]. With the aim of blending the properties of MGs and HEAs, high-entropy metallic glasses (HEMGs) have been developed [11–13]. However, the existence of specific properties of HEMGs as compared to other families of MGs, especially the presence of a high-entropy, sluggish diffusion effect [14] and its effects on the glass-to-liquid transition and the aging and rejuvenation processes, which are essential to control the glassy configuration and adjust the materials properties [11,15], have not been clearly demonstrated.

Dynamic mechanical analysis (DMA) [2], i.e., mechanical spectroscopy, and stress relaxation [16,17] have been proven powerful tools to characterize the dynamics of MGs [17,18]. Stress relaxation has been investigated at different length scales by experiments [16,19] and simulations [20]. Besides, secondary β relaxation, preceding in temperature the collective, large-scale α relaxation, is observed by mechanical spectroscopy and has been associated with local (nanoscale) atomic phenomena [20,21]. Although stress relaxation and mechanical spectroscopy observations are, respectively, the time and frequency domain responses of the same mechanical relaxation phenomenon, direct evidence of the intrinsic correlation between β relaxation and stress relaxation in MGs is still missing.

In this Letter, we present a study of over six different metallic glass formers: three HEMGs and three "conventional" MGs which are representative of the main compositional families of glass-forming alloys. By calorimetric and mechanical tests, we try to step forward in the solving of the following important questions. What is the relation between the thermal activation of liquidlike zones and the relaxation spectrum of metallic glasses? How does the dynamical heterogeneity evolve during changes of the glass state? And, finally, are there systematic dynamical differences between high-entropy and conventional metallic glass formers?

For this purpose, we investigated the stress relaxation behavior of HEMGs and MGs following the stress decay under a constant strain while heating in isothermal steps. The stress decay was monitored for 1800 s in each step from room temperature to the glass transition. It is known that both stress and temperature are equally critical in controlling the stress relaxation dynamics of MGs [22–24], as the external stress reduces the apparent flow activation energy [24]. Here, the applied strains are small and equal

from room temperature to the glass transition, always within 0.3%–0.6%. Within this range the observed behaviors are basically produced by the temperature effects. The selected compositions for this study are three representative HEMGs, $La_{20}Ce_{20}Y_{20}Ni_{20}Al_{20}$ (La-HEMG), $Pd_{20}Pt_{20}Cu_{20}Ni_{20}P_{20}$ (Pd-HEMG) [25] and $Ti_{16.7}Zr_{16.7}Hf_{16.7}Cu_{16.7}Ni_{16.7}Be_{16.7}$ (Zr-HEMG) and three representatives of conventional MGs, $La_{60}Ni_{15}Al_{25}$ (La-MG), $Pd_{40}Ni_{40}P_{20}$ (Pd-MG), and $Zr_{45}Cu_{50}Al_5$ (Zr-MG), with obvious different β relaxation behaviors. As seen in the methods section in Supplemental Material [26] [Figs. S1(a) and S1(b)], all these MGs have a significant supercooled liquid (SCL) region and excellent stability against crystallization. For each composition the tests were performed in both as-quenched samples (cooled from the melt at $\sim 10^5 - 10^6$ K s^{-1}) and relaxed samples (cooled from the SCL at 1.67×10^{-3} K s^{-1}).

The temperature dependence of the normalized loss modulus $E''/E''_{\max}$ obtained by DMA is shown in Figs. 1(a) and 1(b). With a driving frequency of 2 Hz, the maximum of loss modulus $E''_{\max}$, which corresponds to the α relaxation peak, is observed at $T_\alpha = 504$, 588, and 708 K for La-HEMG, Pd-HEMG, and Zr-HEMG and at 488, 602, and 730 K for the La-MG, Pd-MG, and Zr-MG, respectively. The β relaxation is observed as a distinct peak [18,27] for the La-based glasses, a shoulder [17,18] for the Pd-based and an excess wing [28,29], almost merged into the α relaxation, for the two glasses of the Zr family.

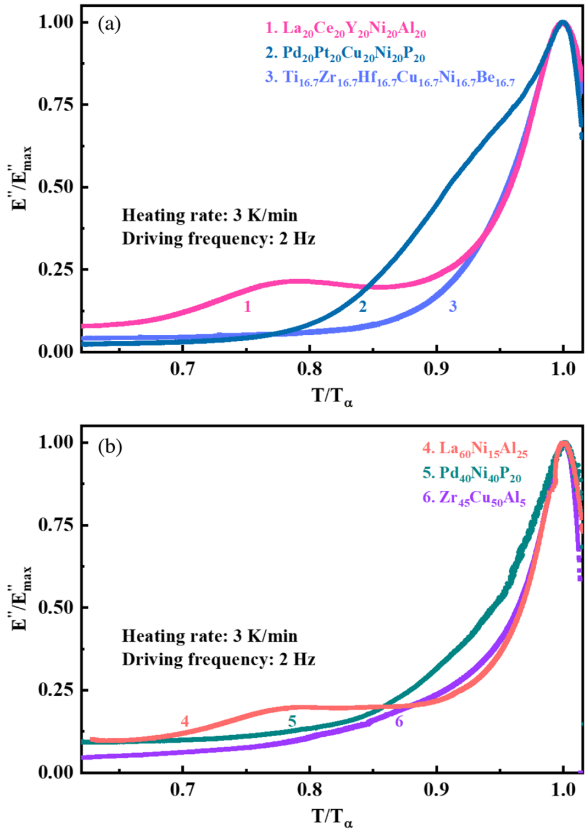

FIG. 1. Normalized loss modulus $E''/E''_{\max}$ as a function of the normalized temperature T/T_α. T_α stands for the peak temperatures of α relaxation probed at 2 Hz. (a) HEMGs (b) conventional MGs.

While crystalline defects and grain boundaries are crucial for the internal friction of crystalline metals [30], the heterogeneous nanoscale structure seems to be the main factor in the case of MGs [31,32]. It has been accepted that MGs can be regarded as viscous, weak-bond regions caged in an elastic, strong-bond matrix, as described by the models based on flow units [33–35] or soft spots [34]. Within this picture, the β relaxation is seen as a reversible process of local atomic rearrangement of these soft spots and it is closely correlated to the mechanical properties of glasses, particularly with the underlying mechanisms of plastic deformation [17,18].

The stress drop of the HEMGs from room temperature to near T_α (for details see the methods section in Supplemental Material [26]) is shown in Figs. 2(a)–2(c). After applying a constant strain, the stress relaxes with time. We define $\delta = [(\sigma_0 - \sigma_r)/\sigma_0]$ as the intensity of stress relaxation, where σ_0 and σ_r are the initial and terminal stresses of each 30 min relaxation curve. The intensity of stress drop δ can be associated to the fraction of liquidlike activated flow units and to viscosity [19,36]. The σ_0 and σ_r of each relaxation curve are depicted as open circles and squares, respectively. One can notice that the decay of σ_0 is not prominent until close to T_g, whereas the decay of σ_r accelerates near T_β (the temperature of the β relaxation) and then drops to zero near T_g. In order to more clearly reveal the influence of the distinct β relaxation behaviors, in Figs. 2(d)–2(f) we depict together the evolution of δ (for 30 min of stress relaxation each 3 K step) and the normalized loss modulus $E''/E''_{\max}$ (driving frequency of 2 Hz and a heating rate of 3 K min^{-1}). With the increase of temperature near T_β, both of these magnitudes accelerate their rising reaching a maximum around T_g. The evolution of δ in the different HEMGs exhibits a hint of a peak for the La-HEMG, a shoulder for Pd-HEMG, and an excess wing for Zr-HEMG, replicating the β relaxations.

Interpreting δ as the fraction of liquidlike activated flow units [19], the increase of δ indicates that a higher fraction of atoms are unfrozen to undergo inelastic deformation [37,38]. This fact can be viewed as the increase of atomic-molecular mobility caused by the thermal activation of microscopic movements. It is interesting to discuss the similarity between the loss modulus and the intensity of stress relaxation. $\delta(T)$ shows the same features as $E''(T)/E''_{\max}$, but shifted to lower temperatures. In this Letter, the driving frequency of DMA experiments was 2 Hz, while the "effective driving frequency" of the stress relaxation tests can be estimated as $f \sim (1/30\ \text{min}) = 6 \times 10^{-4}$ Hz. It is well known that the loss modulus is shifted to low temperatures as frequency decreases [39].

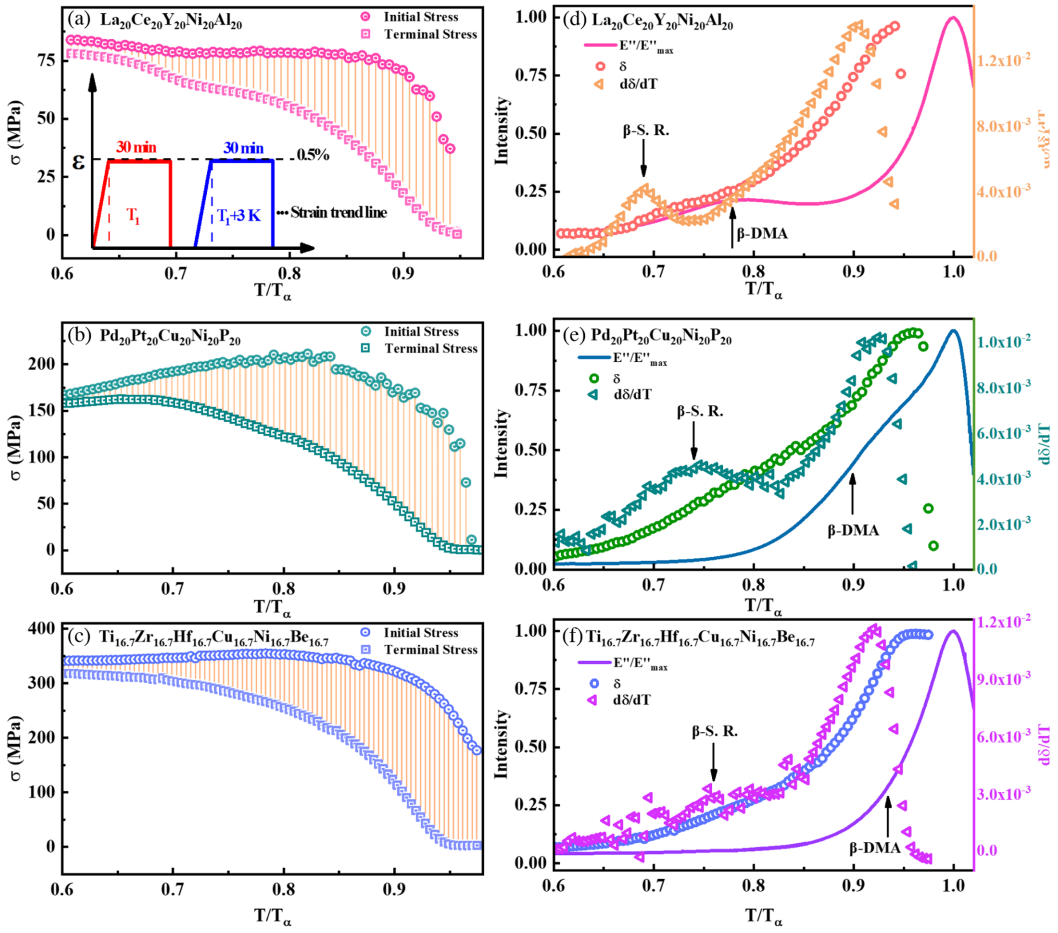

FIG. 2. Stress relaxation measured at stepping temperature from room temperature to T_α for (a) La-HEMG, (b) Pd-HEMG, and (c) Zr-HEMG. Evolution with temperature of stress drop δ, stress drop change rate $d\delta/dT$ and normalized loss modulus $E''/E''_{\max}$ of (d) La-HEMG, (e) Pd-HEMG, and (f) Zr-HEMG.

Following Ref. [19], $\delta(T)$ can be interpreted as the fraction of liquidlike zones, i.e., zones that can relax stress within the duration of the test. Similarly, the integration of the relaxation spectrum obtained by DMA, $\int_0^T [E''(T)/E''_{\max}]dT$, is proportional to the fraction of relaxation modes faster than $\sim f^{-1}$. Therefore, the derivative $d\delta(T)/dT$ should be proportional to $E''(T)/E''_{\max}$ at a frequency of $f \sim 6 \times 10^{-4}$ Hz. Figures 2(d)–2(f) show the behavior of $d\delta(T)/dT$ with clear α and β peaks displaced to lower temperatures, as expected for such a low driving frequency. For all the three materials, the position of the $d\delta(T)/dT$ maximum is found at $\sim 0.9 T_{\alpha,2\ \mathrm{Hz}}$, in agreement with the temperatures at which the slope of the $\tau_c(T)$ (see Fig. 3 and discussion below) is observed to change, indicating the onset of the dynamic glass transition for this frequency. For Pd-HEMG, the α and β become well separated in comparison with the "shoulder" observed at $f = 2$ Hz. For Zr-HEMG, the excess wing observed at $f = 2$ Hz is moved toward lower temperatures and starts to be similar to a broad shoulder of low intensity. The same intrinsic correlation between loss modulus and $d\delta(T)/dT$ can be found in the three conventional La, Pd, and Zr MGs (see Fig. S2 of Supplemental Material [26]). This direct relationship between the fraction of liquidlike zones and the spectrum of relaxation modes is in agreement with the view of MGs being composed by a spatial distribution of zones of different relaxation time [40] or, in other words, more or less liquidlike in nature. The transition from inhomogeneous to homogenous flow is associated to the fraction of liquidlike zones reaching a percolation or threshold fraction of around 25% [19]. Therefore, the results presented here suggest that one could readily establish a way of estimating the inhomogeneous to homogeneous line in a strain-rate–temperature map by integrating the $E''(T)/E''_{\max}$ spectra obtained at different frequencies.

The results in Fig. 2 correspond to as-quenched samples. In this samples, the evolution of liquid-fraction zones is not only due to the activation of the β and α relaxations as temperature increases, but also to the physical aging process (or structural relaxation) occurring during the tests [41]. Physical aging drives the glass to more stable and denser configurations, reducing the excess free volume in

the structure and so also reducing the intensity of the secondary relaxation and the fraction of liquidlike zones. Figure S3 in Supplemental Material [26] show the results of DMA and stress relaxation tests on relaxed samples. The secondary peak in $E''(T)/E''_{\max}$ shows a reduced intensity as expected for well relaxed materials, as now reflects the activation of the β relaxation in a structure with comparatively much less liquidlike zones. For $d\delta(T)/dT$ the peak is clearly reduced, but still evident, for the Pd glasses while it becomes almost indistinguishable for the La systems. The same effect is observed in calorimetry (see Fig. S4) where the activation of the β relaxation shows a clear signature in Pd systems while it is negligible in La based. This suggests a different nature of the secondary relaxation in Pd and La systems. It can be correlated to the increase of the liquidlike volume fraction in Pd, whereas in La systems it seems to be related to an isolated mobility mechanism which remains too fast to contribute to the overall stress relaxation at longer times.

In order to further characterize the relaxation behavior of the glasses, the stress relaxation curves at each temperature step were fitted to the phenomenological Kohlrausch-Williams-Watts (KWW) equation [19,42]

$$\sigma(t) = \sigma_0 \exp\left(-\frac{t}{\tau_c}\right)^{\beta_{\mathrm{KWW}}}, \tag{1}$$

where $\sigma(t)$ is the stress at time t, β_{KWW} is a stretching exponent, a parameter linked to the dynamic heterogeneity, and τ_c is the stress relaxation timescale. Some selected results are shown in Fig. 3. Figures S5–S7 in Supplemental Material [26] show the relaxation curves at various temperatures and details of the corresponding fittings with Eq. (1). Figure S8, show the results for the La, Pd, and Zr-MGs.

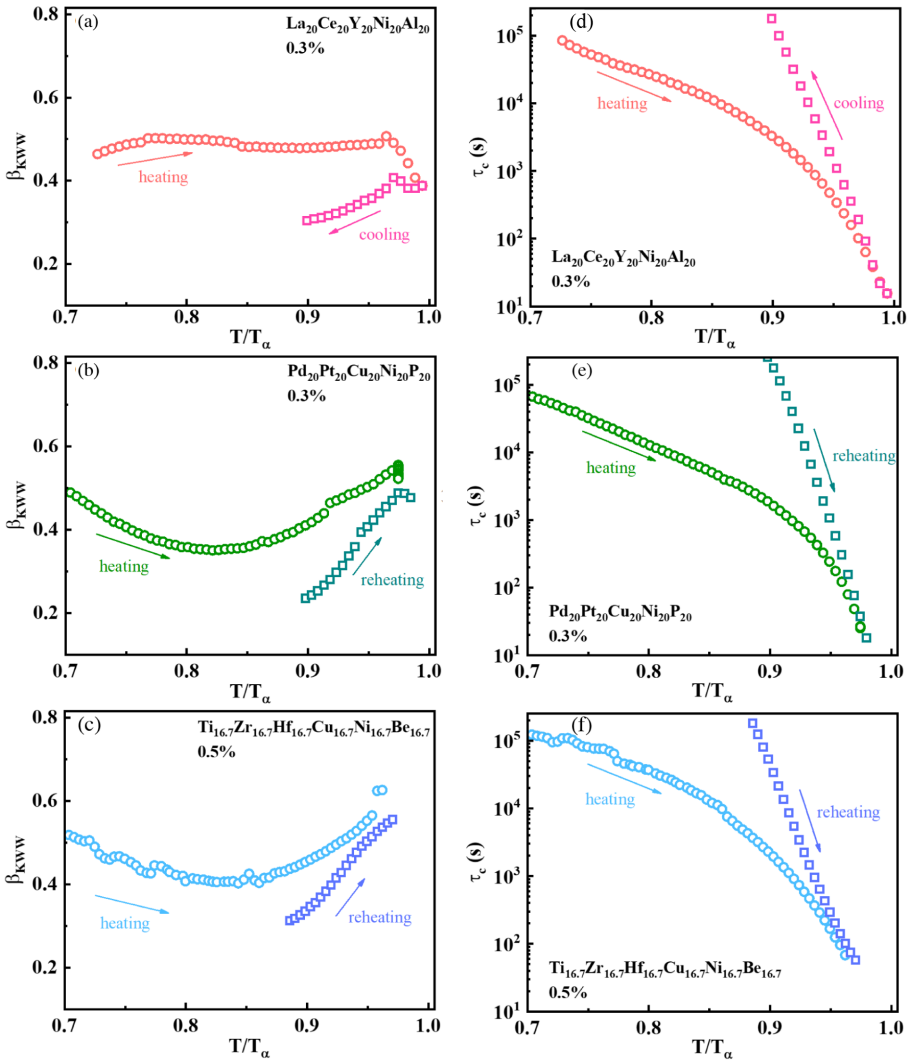

FIG. 3. The fitted KWW parameters β_{KWW} of (a) La-HEMG, (b) Pd-HEMG, and (c) Zr-HEMG and τ_c (d) La-HEMG, (e) Pd-HEMG, and (f) Zr-HEMG with initial as-quenched state and with well relaxed state (second cycle of stress relaxation measurements after slowly cooling from T_g).

The overall behavior is similar for all the alloys. At $T/T_\alpha < 0.7$ the stress relaxation achieved during 30 min is small, less than 15%. This indicates that the relaxation timescale is much longer than the experimental time window. For the relaxed samples, this happens until $T/T_\alpha \lesssim 0.85$ due to the reduction of liquidlike zones in the more densified state. The results in this low temperature range are not shown in Fig. 3 and will not be discussed here as a longer experimental relaxation step would be necessary to properly characterize τ_c and β_{KWW}. In the temperature region $0.7 < T/T_\alpha < 0.9$, $\tau_c(T)$ decreases with temperature, going from values above 10^4 s toward a value of $\tau_c \sim 10^3$ s at $T/T_\alpha \sim 0.9$. The parameter β_{KWW} varies within 0.35 to 0.6, which are typical values in the relaxation of amorphous alloys [19,27,43,44].

The physical aging of the glasses during the tests seems reflected on the behavior of $\beta_{\mathrm{KWW}}(T)$. Although aging drives the system to a lower energy state with less overall internal friction [39], various recent studies have shown that the underlying relaxation time distribution becomes more heterogeneous during aging [16,44–46]. Thus, although the total intensity of stress relaxation is smaller in the aged samples, the different timescales participating in it become more separated as indicated by a decrease of $\beta_{\mathrm{KWW}}(T)$. This phenomenon is also observed here in the temperature range going from $T/T_\alpha = 0.7$ to 0.8. The as-quenched samples start with a $\beta_{\mathrm{KWW}}(T) \sim 0.5$, a level of dynamical heterogeneity similar to what is observed in the SCL [47]. As soon as the fraction of activated liquidlike zones increases, the aging process is allowed to proceed, and $\beta_{\mathrm{KWW}}(T)$ decreases until values around 0.3, as it was also observed for very well aged glassy states in other works [16,44,45]. At the higher temperatures, the transition from a relaxed glass toward the liquid state shows, in parallel, the increase of the fraction of liquidlike zones and the $\beta_{\mathrm{KWW}}(T)$ parameter, which returns to values in the range 0.5–0.6 at the glass transition. The reason of the more constant behavior of $\beta_{\mathrm{KWW}}(T)$ in the La-HEMG and MG (see Fig. S3) is not clear but may be related to the presence of a distinct secondary process that dominates the atomic mobility at the temperature range $T/T_\alpha = 0.7$–0.8. It is worth noticing that the evolution of $\beta_{\mathrm{KWW}}(T)$ [shown in Figs. 3(b) and 3(c)] seems to be concave regardless of the material state. The preannealed and well-relaxed samples show also a striking concave nature (see Fig. S9). However, the duration of the isothermal steps of the experiments presented in this Letter is not long enough to conclusively study the behavior of relaxed samples at low temperatures.

At $T/T_\alpha \sim 0.9$, the relaxation times of the six glasses are of the same timescale as the isothermal steps (2100 s); this allows the glasses to get closer to an ergodic state within each temperature step. This is observed by the progressive change of the slope of $\tau_c(T)$, which signals the transition from glass to SCL dynamics. Accordingly, between $0.9 < T/T_\alpha < 0.95$ the relaxation dynamics are more accelerated by the increase of temperature. At $T/T_\alpha \sim 0.93$–0.94, all materials achieve full relaxation during the 30 min tests. Finally, above this temperature, the onset of crystallization is clearly detected in the shape of the relaxation curves, thus also dictating the upper limit of the validity of the KWW equation to describe the experimental data (see Figs. S5–S7).

Finally, we will discuss the intrinsic effect of high entropy in the glass and liquid dynamics. The difference of specific heat between the glassy alloys and the crystalline baselines was measured by differential scanning calorimetry. The $c_p(T)$ curves are given in Fig. S4 in Supplemental Material [26]. Figures 4(a)–4(c) and 4(g) show the step $\Delta c_{p,T_g} = c_{p,l} - c_{p,g}$ at the glass transition and the integration $\Delta S_{lg-x} = \int_{T_1}^{T_2} \{[c_{p,lg}(T) - c_{p,x}(T)]/T\} dT$, which corresponds to the excess of entropy between the amorphous (glass and liquid) and the crystallized samples. It can be observed that the HEMGs systematically show higher glass transition steps $\Delta c_{p,T_g}$ and configurational entropies in comparison with the conventional MGs.

The mobility in the glass is determined by both the aging process and the fast part of the relaxation spectrum, dominated by the β relaxation and the high-frequency wing of the α process. The specific shape of this spectrum is primarily dependent on the kind of metallic glass family, independently of the high-entropy or conventional nature of the alloys. Interestingly, the value $E_\beta/RT_g \approx 25 + 2$ (see Supplemental Material, Table S1 [26]) derived from stress relaxation is consistent with the empirical relationship $E_\beta/RT_g \approx 26$ found in various MGs [17,18], in agreement with previous dynamic mechanical analyses [48] and amplitude-modulation atomic force microscopy results [49]. On the other hand, the relaxation tests performed in this Letter, allow us to study the temperature evolution of the dynamics in the region of the glass transition, dominated by the α (or viscous) relaxation. Figures 4(d)–4(f) show the evolution with temperature of τ_c in the region where it becomes shorter than 300 s. The fragility of the liquid $m = [d(\log \tau_c)/d(T_g/T)]$, or equivalently, the apparent activation energy of the relaxation E_α, can be calculated in this region. It is found that the HEMGs show always a stronger liquid behavior than their MGs counterparts. At the same relative temperatures with respect to the glass transition, the Pd and La HEMGs show slower dynamics than their corresponding conventional counterparts.

Configurational and vibrational entropy contribute to the total entropy of metallic glasses [50–52]. The vibrational entropy in MGs (and their undercooled liquids) is approximately equal to that of the corresponding crystals [50,53], and this implies that the excess entropy of MGs can be mainly attributed to the configurational entropy difference [51,53]. The rough correlation usually observed in glass formers between the Δc_p step at the glass transition and the

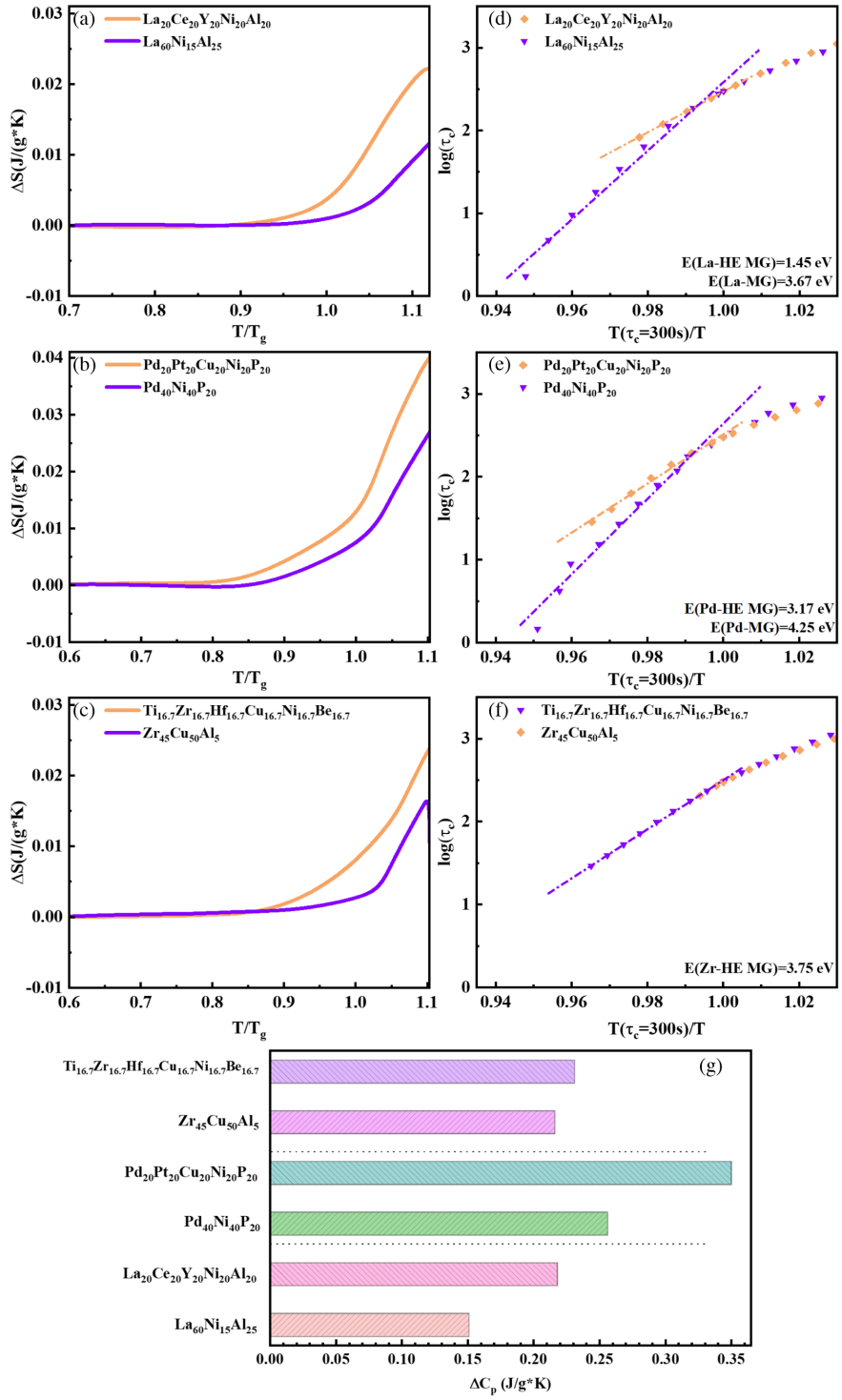

FIG. 4. The excess of entropy ΔS of (a) La-based, (b) Pd-based, and (c) Zr-based HEMGs and MGs. Stress relaxation time τ_c vs reciprocal temperature $T(\tau_c = 300\ \mathrm{s})/T$ and fitted Arrhenius plots for (d) La-based, (e) Pd-based, and (f) Zr-based HEMGs and MGs. (g) The step Δc_p at the glass transition of well relaxed samples of HEMGs and MGs.

liquid fragility is not fulfilled for the studied alloys and this can be another trait related to the high-entropy effect. The larger Δc_p of the HEMGs indicates that, in these alloys, the glass to liquid transition unfreezes the possibility to explore a larger quantity of configurations [54]. However, this is not correlated to faster dynamics (or a more fragile liquid behavior) but to the high entropy of mixing of these compositions. This points toward the sluggish diffusion high-entropy effect in the liquid dynamics as suggested in other works [14,55,56].

In summary, the evolution of stress relaxation of high entropy and conventional MGs with different types of β processes was investigated. The study of the timescale and shape of the relaxation curves indicates that HE MGs tend to have an enhanced strong liquid behavior above the dynamic glass transition, and that aging of the glass increases the relative separation of the relaxation times contributing to the stress relaxation, as reflected in the decrease of the β_{KWW} exponent. Importantly, this Letter shows that the fraction of zones that behave liquidlike during a fixed time interval is proportional to the relaxation mode spectrum at the corresponding low frequency. Our results shed light on the intrinsic correlation between the static and dynamic mechanical response in high-entropy and conventional metallic glasses, and they provide a practical guideline for understanding, and subsequently controlling, the mechanical behavior of HE MGs.

This work is supported by the NSFC (Grant No. 51971178), the Fundamental Research Funds for the Central Universities (Grant No. D5000220034), the Natural Science Basic Research Plan for Distinguished Young Scholars in Shaanxi Province (Grant No. 2021JC-12). E. Pineda and D. Crespo acknowledge financial support from the research project PID2020–112975GB-I00 funded by MCIN/AEI/10.13039/501100011033 and from Generalitat de Catalunya (AGAUR Grant No. 2017SGR 0042). Y. J. Wang was financially supported by NSFC (Grant No. 12072344) and the Youth Innovation Promotion Association of the Chinese Academy of Sciences. Y. Yang acknowledges financial support from Research Grant Council (RGC), the Hong Kong government through the General Research Fund (GRF) with Grants No. City U11200719 and No. CityU11213118. Y. J. Duan is sponsored by the Innovation Foundation for Doctor Dissertation of Northwestern Polytechnical University (No. CX202031) and China Scholarship Council (CSC) under Grant No. 202006290092.

*Corresponding author.
qjczy@nwpu.edu.cn
†Corresponding author.
eloi.pineda@upc.edu

[1] J. Schroers and W. L. Johnson, Phys. Rev. Lett. **93**, 255506 (2004).
[2] W. H. Wang, Prog. Mater. Sci. **106**, 100561 (2019).
[3] M. R. Chellali, S. H. Nandam, and H. Hahn, Phys. Rev. Lett. **125**, 205501 (2020).
[4] A. D. Phan, A. Zaccone, V. D. Lam, and K. Wakabayashi, Phys. Rev. Lett. **126**, 025502 (2021).
[5] D. B. Miracle, Nat. Commun. **10**, 1805 (2019).
[6] S. Wei, S. J. Kim, J. Kang, Y. Zhang, Y. Zhang, T. Furuhara, E. S. Park, and C. C. Tasan, Nat. Mater. **19**, 1175 (2020).
[7] X. Chang, M. Zeng, K. Liu, and L. Fu, Adv. Mater. **32**, 1907226 (2020).
[8] D. B. Miracle and O. N. Senkov, Acta. Mater. **122**, 448 (2017).
[9] E. P. George, D. Raabe, and R. O. Ritchie, Nat. Rev. Mater. **4**, 515 (2019).
[10] P. Koželj, S. Vrtnik, A. Jelen, S. Jazbec, Z. Jagličić, S. Maiti, M. Feuerbacher, W. Steurer, and J. Dolinšek, Phys. Rev. Lett. **113**, 107001 (2014).
[11] W. H. Wang, JOM **66**, 2067 (2014).
[12] E. Goncharova, R. Konchakov, A. Makarov, N. Kobelev, and V. Khonik, J. Phys. Condens. Matter **29**, 305701 (2017).
[13] H. W. Luan, X. Zhang, H. Y. Ding, F. Zhang, J. H. Luan, Z. B. Jiao, Y. C. Yang, H. T. Bu, R. B. Wang, J. L. Gu, C. L. Shao, Q. Yu, Y. Shao, Q. S. Zeng, N. Chen, C. T. Liu, and K. F. Yao, Nat. Commun. **13**, 2183 (2022).
[14] J. Jing, Z. Lu, J. Shen, T. Wada, H. Kato, and M. Chen, Nat. Commun. **12**, 3843 (2021).
[15] C. A. Schuh, T. C. Hufnagel, and U. Ramamurty, Acta. Mater. **55**, 4067 (2007).
[16] P. Luo, P. Wen, H. Y. Bai, B. Ruta, and W. H. Wang, Phys. Rev. Lett. **118**, 225901 (2017).
[17] H. B. Yu, K. Samwer, Y. Wu, and W. H. Wang, Phys. Rev. Lett. **109**, 095508 (2012).
[18] H. B. Yu, X. Shen, Z. Wang, L. Gu, W. H. Wang, and H. Y. Bai, Phys. Rev. Lett. **108**, 015504 (2012).
[19] Z. Wang, B. Sun, H. Bai, and W. Wang, Nat. Commun. **5**, 5823 (2014).
[20] Y. Sun, S. X. Peng, Q. Yang, F. Zhang, M. H. Yang, C. Z. Wang, K. M. Ho, and H. B. Yu, Phys. Rev. Lett. **123**, 105701 (2019).
[21] G. P. Johari and M. Goldstein, J. Chem. Phys. **53**, 2372 (1970).
[22] P. Guan, M. Chen, and T. Egami, Phys. Rev. Lett. **104**, 205701 (2010).
[23] H. B. Yu, R. Richert, R. Maaß, and K. Samwer, Phys. Rev. Lett. **115**, 135701 (2015).
[24] Y. C. Wu, B. Wang, Y. C. Hu, Z. Lu, Y. Z. Li, B. S. Shang, W. H. Wang, H. Y. Bai, and P. F. Guan, Scr. Mater. **134**, 75 (2017).
[25] Y. J. Duan, J. C. Qiao, T. Wada, H. Kato, Y. J. Wang, E. Pineda, and D. Crespo, Scr. Mater. **194**, 113675 (2021).
[26] See Supplemental Material at http://link.aps.org/supplemental/10.1103/PhysRevLett.129.175501 for the details about sample preparation, dynamic-mechanical and stress relaxation experiments.
[27] J. C. Qiao, Q. Wang, J. M. Pelletier, H. Kato, R. Casalini, D. Crespo, E. Pineda, Y. Yao, and Y. Yang, Prog. Mater. Sci. **104**, 250 (2019).
[28] J. C. Qiao, Y. Yao, J. M. Pelletier, and L. M. Keer, Int. J. Plast. **82**, 62 (2016).
[29] L. T. Zhang, Y. J. Duan, T. Wada, H. Kato, J. M. Pelletier, D. Crespo, E. Pineda, and J. C. Qiao, J. Mater. Sci. Technol. **83**, 248 (2021).
[30] T. S. Kê, Scr. Metall. Mater. **24**, 347 (1990).
[31] S. D. Feng, L. Qi, L. M. Wang, P. F. Yu, S. L. Zhang, M. Z. Ma, X. Y. Zhang, Q. Jing, K. L. Ngai, A. L. Greer, G. Li, and R. P. Liu, Scr. Mater. **115**, 57 (2016).
[32] D. Wei, J. Yang, M. Q. Jiang, B. C. Wei, Y. J. Wang, and L. H. Dai, Phys. Rev. B **99**, 014115 (2019).
[33] T. Ichitsubo, E. Matsubara, T. Yamamoto, H. S. Chen, N. Nishiyama, J. Saida, and K. Anazawa, Phys. Rev. Lett. **95**, 245501 (2005).

[34] W. H. Wang, Prog. Mater. Sci. **57**, 487 (2012).
[35] X. Bian, G. Wang, Q. Wang, B. Sun, I. Hussain, Q. Zhai, N. Mattern, J. Bednarčík, and J. Eckert, Mater. Res. Lett. **5**, 284 (2017).
[36] J. D. Ferry, *Viscoelastic Properties of Polymers* (John Wiley & Sons, New York, 1980).
[37] H. Wagner, D. Bedorf, S. Küchemann, M. Schwabe, B. Zhang, W. Arnold, and K. Samwer, Nat. Mater. **10**, 439 (2011).
[38] S. G. Mayr, Phys. Rev. Lett. **97**, 195501 (2006).
[39] Y. J. Duan, D. S. Yang, J. C. Qiao, D. Crespo, J. M. Pelletier, L. Li, K. Gao, and T. Zhang, Intermetallics **124**, 106846 (2020).
[40] B. Shang, J. Rottler, P. Guan, and J. L. Barrat, Phys. Rev. Lett. **122**, 105501 (2019).
[41] E. Pineda, P. Bruna, B. Ruta, M. Gonzalez Silveira, and D. Crespo, Acta. Mater. **61**, 3002 (2013).
[42] G. Williams and D. C. Watts, Trans. Faraday Soc. **66**, 80 (1970).
[43] J. C. Qiao, Y. J. Wang, L. Z. Zhao, L. H. Dai, D. Crespo, J. M. Pelletier, L. M. Keer, and Y. Yao, Phys. Rev. B **94**, 104203 (2016).
[44] N. Amini, F. Yang, E. Pineda, B. Ruta, M. Sprung, and A. Meyer, Phys. Rev. Mater. **5**, 055601 (2021).
[45] D. Soriano, H. Zhou, S. Hilke, E. Pineda, B. Ruta, and G. Wilde, J. Phys. Condens. Matter **33**, 164004 (2021).
[46] Y. J. Lü, C. C. Guo, H. S. Huang, J. A. Gao, H. R. Qin, and W. H. Wang, Acta. Mater. **211**, 116873 (2021).
[47] L. M. Wang, R. Liu, and W. H. Wang, J. Chem. Phys. **128**, 164503 (2008).
[48] J. Hachenberg, D. Bedorf, K. Samwer, R. Richert, A. Kahl, M. Demetriou, and W. Johnson, Appl. Phys. Lett. **92**, 131911 (2008).
[49] F. Zhu, H. K. Nguyen, S. X. Song, D. P. B. Aji, A. Hirata, H. Wang, K. Nakajima, and M. W. Chen, Nat. Commun. **7**, 11516 (2016).
[50] G. P. Johari, J. Chem. Phys. **112**, 7518 (2000).
[51] D. Han, D. Wei, J. Yang, H. L. Li, M. Q. Jiang, Y. J. Wang, L. H. Dai, and A. Zaccone, Phys. Rev. B **101**, 014113 (2020).
[52] M. Goldstein, J. Chem. Phys. **64**, 4767 (1976).
[53] H. L. Smith, C. W. Li, A. Hoff, G. R. Garrett, D. S. Kim, F. C. Yang, M. S. Lucas, T. Swan Wood, J. Y. Y. Lin, M. B. Stone, D. L. Abernathy, M. D. Demetriou, and B. Fultz, Nat. Phys. **13**, 900 (2017).
[54] L. M. Martinez and C. A. Angell, Nature (London) **410**, 663 (2001).
[55] M. H. Tsai and J. W. Yeh, Mater. Res. Lett. **2**, 107 (2014).
[56] J. W. Yeh, Ann. Chim. Sci. Mat. **31**, 633 (2006).